International Journal of Mechanical, Industrial and Aerospace Sciences
ISSN: 2517-9950
Vol:6, No:8, 2012

Alternative Approach in Ground Vehicle Wake Analysis

L. Sterken, S. Sebben, L. Löfdahl

***Abstract*—**In this paper an alternative visualisation approach of the wake behind different vehicle body shapes with simplified and fully-detailed underbody has been proposed and analysed. This allows for a more clear distinction among the different wake regions. This visualisation is based on a transformation of the cartesian coordinates of a chosen wake plane to polar coordinates, using as filter velocities lower than the freestream. This transformation produces a polar wake plot that enables the division and quantification of the wake in a number of sections. In this paper, local drag has been used to visualise the drag contribution of the flow by the different sections. Visually, a balanced wake can be observed by the concentric behaviour of the polar plots. Alternatively, integration of the local drag of each degree section as a ratio of the total local drag yields a quantifiable approach of the wake uniformity, where different sections contribute equally to the local drag, with the exception of the wheels.

***Keywords*—**Coordinate transformation, ground vehicle, local drag, wake.

I. Introduction

With the increasing fuel prices and the more strict requirements in CO_2 exhaust levels, vehicle manufacturers are investigating intensively in methods to reduce the energy consumption of vehicles. Since aerodynamics plays an important role in the total driving resistance of vehicles, it is a logical step to focus in this area.

A large part of the aerodynamic air resistance of bluff bodies can be contributed to the pressure drag caused by its wake, see [1], [5], [7] and [11]. Therefore, a better understanding of the flow structures in the wake is a necessity in order to develop methods for drag reduction. Numerous investigations on ground vehicle models have been conducted.

Reference [7], for example, has investigated the different flow structures that are present in the near-wake of an automotive bluff body and characterised them with respect to vehicle type. Reference [9] introduced a new aerodynamic approach with the fluid tail technique (FTT) to search for a more balanced wake. Conditions required for a balanced wake are a circular or elliptical perimeter of the base, the flow separation had to be as close to the perimeter of the base as possible and it had to be transversal with respect to the vehicle's motion of direction. However it is well-known that a vehicle's wake does not reach this elliptical or circular cross-section, mainly due to wake interaction between wheel/wheelhouse wake and base wake [10].

L. Sterken is with the Environment & Fluid Dynamics Center, Volvo Car Corporation, Göteborg, Sweden (e-mail: lsterken@volvocars.com).

S. Sebben, PhD is with the Environment & Fluid Dynamics Center, Volvo Car Corporation, Göteborg, Sweden. She is also with the Department of Applied Mechanics, Chalmers University Of Technology. (e-mail: ssebben@volvocars.com).

Prof. L. Löfdahl is with the Department of Applied Mechanics, Chalmers University of Technology, Göteborg, Sweden.

Starting with the momentum and continuity equations, an expression for the drag as a fucntion of the pressure and velocities in the wake of bluff bodies can be derived. This derivation can be found in a number of references, as [2], [3], [5] and [11]. Examples where local drag has been used to visualise the air resistance in the flow are [6], [8] and [10]. Reference [8] calls this expression microdrag. This paper prefers the term local drag since the flow properties are still determined on a macroscopic scale. In order to calculate the local drag, the primitive variables pressure and velocity at a plane 100 mm behind the vehicle body are exported for post-processing. In this study it has been chosen as definition of the wake size to follow the characteristic wake parameter, velocity deficit U_D, usually used in axisymmetrical body wake analysis as a measure for the wake width [12]. The velocity deficit is defined by the difference between freestream and local velocity $U_\infty - U$. Reference [13] uses this parameter in his analysis for the far-field wake of bluff bodies to determine the wake size, but chooses to define the size in terms of half widths, which can be seen as the distance between points where the velocity deficit has reduced to half its maximum value. Here, it is opted to determine the wake size simply as the region where there is a velocity deficit. It is thought this is beneficial to investigate the uniformity of the wake since this definition incorporates more information into the wake analysis.

Eventhough a vehicle's wake does not obtain an elliptical or circular cross-section, this paper will introduce a coordinate transformation of the wake region into polar coordinates and rescale it to a unity circle. The main intention for this approach is to obtain a better insight in where the wake can be optimised with drag reduction as goal. Another aim is to facilitate the division of the wake into distinct zones that allows for their quantification. This quantification can then be used to identify and measure the main sources to the air resistance. The present analysis conducted in this paper has been for two vehicle types, an SUV and a sedan type, and for different underbody complexities.

II. Methodology

This section describes the applied methodology used to analyse the results. In Section II-A the different configurations that are investigated are explained. Section II-B describes in detail the numerical setup used for the CFD simulations. Finally, Section II-C explains the post-processing steps consisting of the coordinate transformation to polar coordinates and the definition of local drag.

A. Configurations

Three levels of geometric complexity of the models have been considered.

They can be classified as:

1. *Simplified models:* The concept of coordinate transformation has initially been applied on a simplified model of a SUV-type vehicle with no wheels nor wheelhouses.

Fig. 1 gives a surface representation of this simplified vehicle geometry.

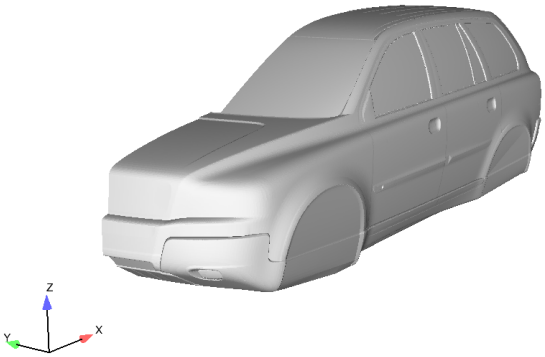

Fig. 1 Isometric view of the simplified model

Three configurations have been chosen to analyse the wake in polar format. The configurations have a difference in drag coefficient C_D as seen in Table I.

The exterior of the vehicle remains unchanged. The modifications are done on the underbody shape and on the rear ground clearance (defined as the distance from the ground to the rear axle). The front ground clearance (defined as the distance from the ground to the engine undershield) remains constant and is for all configurations lower than the rear ground clearance. These simple configurations resulted in drag changes with reasonable magnitude to be captured in the proposed coordinate transformation to polar plots and hence allow a judgment of the benefits of such an approach. Fig. 2 shows a longitudinal profile of the three configurations.

2. *Semi-detailed models:* Three different sedan vehicles have been investigated with a simplified flat underbody. These models have about the same dimensions, but they differ in design language. The models have wheels and wheelhouses with the wheels of the same type and size on all three models. Fig. 3 shows an example of sedan 3 with a flat underbody.

TABLE I
ΔC_D SIMPLIFIED MODELS

Configurations	ΔC_D
Ref	0.000
A	-0.003
B	0.009

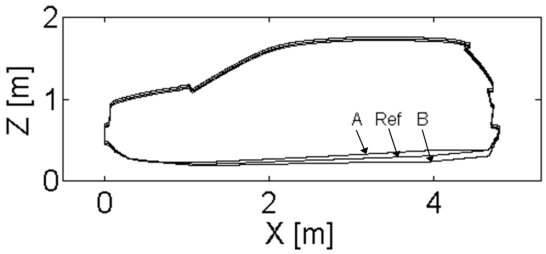

Fig. 2 Simplified model profiles

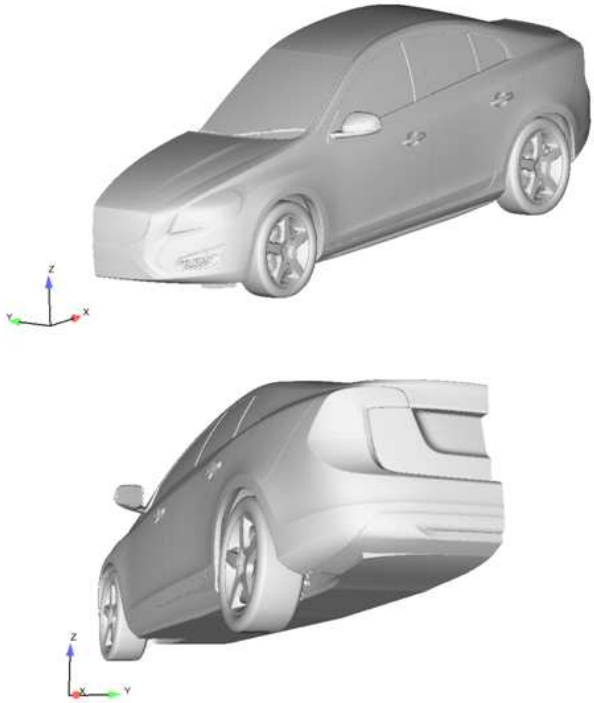

Fig. 3 Semi-detailed model

3) *Detailed model:* A sedan model with a fully detailed underbody has been investigated and compared with the same sedan model with a flat underbody. This sedan has the same exterior as sedan 3, but with a fully detailed underbody, as can be seen in Fig. 4.

B. Numerical setup

All numerical simulations have been conducted following the in-house CFD guidelines at Volvo Car Corporation. The geometry data was prepared in ANSA, meshed in Harpoon and solved using Fluent. Only the left side of the models was meshed and simulated while using a symmetry plane at the centerline of the vehicle.

The simulations were performed in steady – state with the realizable k – eps model and standard wall function.

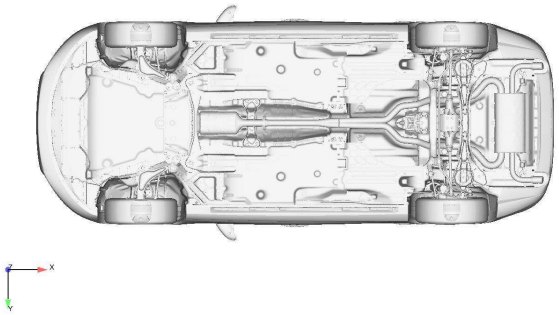

Fig. 4 Detailed model

The moving ground was modeled using a translational boundary condition and the wheels were modeled using a combination of a rotational boundary condition and a Moving Reference Frame (MRF) region.

C. Post – processing

After convergence has been reached, the flow information - the pressure and the three velocity components - in all node points of the YZ-plane 100 mm behind the vehicle is exported to a text file. This file is then further postprocessed in Matlab. Using a cartesian plot of a simplified model wake plane, the process steps can be divided into the following, with respect to Fig. 5 (note that the colouring has been altered to make the regions of interest more visible):

- Find the node point with minimum longitudinal velocity, V_x (Point 1),
- Project Point 1 onto the symmetry line, resulting in Point 2, which will function as origin for coordinate transformation to polar coordinates, (r,θ),
- Transform the cartesian coordinates of all node points to polar coordinates with respect to the point of origin, Point2,
- Filter out the node points with a velocity lower than 99% of the freestream velocity,
- Scale the filtered node points to a unity circle according to $\frac{r(\theta)}{r_{\max}(\theta)}$.

Since symmetry is used in the simulations with only half a vehicle model, the result is a half wake, of which the transformation from a cartesian to a polar plot results in a wake defined between an angle 90º and 270º.

As mentioned in Section I, the definition of the wake size is based on a velocity less than the freestream velocity. This has been done out of practical considerations since it facilitates the separation of the points of interest from all the points of the wake plane. An approach with a total pressure coefficient equal to 1 also has been considered, but this approach takes the first layer of points close the ground into account, complicating the distinction of the vehicle model wake near the ground (most noticeable with the wheel wake).

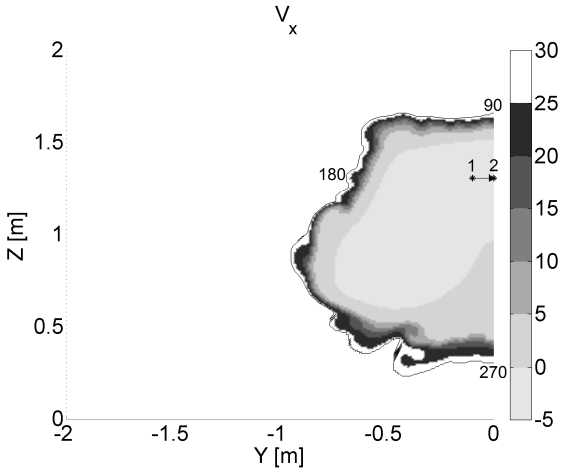

Fig. 5 Step process for coordinate transformation

The boundary of $V = 0.99V_\infty$ is visualised in the cartesian plots by a black contourline around the wake. In the polar plots this is visualised by the radius equal to 1 of the unity circle.

With the flow information for each point, the local drag integrated over the wake area S can be calculated as a function of the total pressure coefficient cptot, the x – component of the velocity V_x, the y – component of the velocity V_y, the z – component of the velocity V_z and the freestream velocity V_∞.

This equals the drag coefficient C_D multiplied with the projected frontal area S. The expression is given in (1), [5] and [11]

$$C_D A = \int_S (1 - c_{p_{tot}})dS - \int_S \left(1 - \frac{V_x}{V_\infty}\right)^2 dS + \int_S \frac{V_y^2 + V_z^2}{V_\infty^2} dS \quad (1)$$

The local drag is an indicator for the location of air resistance contribution in the flow. Regions of high drag can be visualised this way. Further insight and similar definitions can be found in [5] and [11]. The first term in 1 is the total pressure loss which accounts for about 80% of the total drag. The second term is the longitudinal velocity deficit, but its contribution is usually negligeable. The last term is the vortex drag (or sometimes also called induced drag) and is responsible for about 20% of the total drag.

III. Results

This chapter shows the wake of the different vehicle models studied after the polar coordinate transformation and compares the results with the cartesian plots. These polar plots will then be used to calculate the contribution of each pie section as a ratio to the total local drag contribution of the polar plot. This approach will be first discussed for a simplified model, next for a semi-detailed model and finally for a fully detailed model. Details regarding these models have been explained in Section II-A.

A. Simplified models

Table I shows the C_D-values of the three simplified models, discussed in Section II-A.

Model A produced the lowest drag, while model B had the highest air resistance. In Fig. 6 the cartesian and polar plots are given side-by-side for each of the three configurations. Observing these plots, similarities between the different configurations can be found. These similarities make it possible to divide the polar plot in different sections. The first similarity can be observed between 135º and 155º. A discontinuity accompanied with a local drag area increase can be seen that is resulting from the D-pillar. For configuration A, this discontinuity is not as visible as for the other two configurations. The second similarity can be seen at 190º where a local drag bulge appears from the exterior catwalk. Between 210º and 220º the layer with high local drag is at its thinnest. This is where the flow experiences a strong inward and upward acceleration, starting where side and underbody flow meet and move into the low pressure region behind the vehicle.

As mentioned in Section II-C, the boundary for the wake is set up such that the velocity is 99% of the freestream velocity. Under these conditions, a higher local drag near the boundary, such as seen in configuration B, means that the wake area is larger, subsequently delaying the pressure recovery. The boundary is well within the mixing shear layer. In Ref and configuration A, the lower local drag indicates a better pressure recovery due to a smaller wake area. Here, the boundary is situated at the outside of the shear layer with a total pressure coefficient close to 1 and the velocity vector mostly determined by its x-component. Configuration B presents a stronger upwash from the underbody increasing the induced drag and hence local drag from the underbody towards the point of origin (Point 2 in Fig. 5).

B. Simplified models

Similar to the simplified models just described the wake zone of the semi-detailed models in polar plots can be divided in different zones. For each sedan, the corresponding ΔC_D – value can be found in Table II.

TABLE II
ΔC_D SEMI-DETAILED SEDAN MODELS

Model	ΔC_D
Sedan 1	0.000
Sedan 2	-0.001
Sedan 3	0.016

Fig. 7 shows the cartesian and the polar plots for the three models. The wake zones of all sedans have a distinct bulge between 135º and 160º that results from the side mirror wake interacting with the C-pillar vortices. Between 200º and 250º the wheel wake shows in the polar plots by bending the contour lines inwards towards the center of the polar plot. For sedan 2 and sedan 3, the C-pillar wake is positioned at an angle of 120º. For sedan 1, the C-pillar wake is positioned closer to the top symmetry region at 90º.

The remaining regions are in counterclockwise direction- the top region, the side region and the underbody region. This confirms the polar plots have the ability to visualise the main flow structures that are also visible in the cartesian plots.

However the polar plot facilitates the division of the wake into zones associated with the different flow structures. This way, a division of the wake can be maked into a top region from 90º to 160º, a side region from 160º to 200º, a wheel wake region from 200º to 250º and an underbody region from 250º to 270º. Sedan 3 has a higher local drag near the boundary compared to the other sedan models. The high local drag near the boundary indicates a lower pressure recovery since the wake area remains high. For all three cars the wheel wake region, that interacts with the ground, generates a velocity deficit and hence increases the local drag near the boundary immediate to the ground. All three cars have a good pressure recovery from the underbody, seen by the lower local drag near the boundary. However Sedan 1 and Sedan 3 have a stronger upwash increasing in turn the induced drag part of the local drag.

With the data given in the polar definition described through this paper, additional representations can be calculated by integrating the local drag for each degree of the polar plot and compare it to the total local drag over the whole wake. Fig. 8 shows this local drag ratio of each degree – section. The parallel line represents an equal local drag distribution of each degree over the 180 degrees. Sedan 1 shows three main peaks of contributions to the local drag. These peaks represent the wheel wake area (from 200º to 250º), the side mirror area (from 135º to 160º) and the flow from the top section close to the symmetry plane (around 90º). A much lower than average contribution comes from the side. This corresponds to a low interaction between the wheel wake and the side region wake, which is a desirable feature in vehicle aerodynamics. Sedan 2 shows two even more pronounced peaks from the wheel area, a smaller drag contribution from the C-pillar vortices (from 110º to 125º), and similar to sedan 1, a contribution of side mirror wake. Sedan 2 contributes more to the wake drag in the side region compared to sedan 1, but has a much lower contribution in the underbody region from 250º to 270º). Sedan 3 has much less pronounced peaks indicating that the drag is not only coming from the known drag sources like the wheels, for example. There is almost no distinction between the drag contribution resulting from the side region and the wheel wake region. This shows a strong flow interaction between the two regions. Similarly the wheel wake region and underbody region show a strong connection, which is not desirable. It is understood that a less clear distinction of the wheels is actually a negative sign for a balanced wake structure.

C. Detailed models

The semi – detailed sedan 3 model explained in Section II-A is compared with a detailed model of the same car. In Table III the ΔC_D – value of the detailed model relative to the semi – detailed model is given.

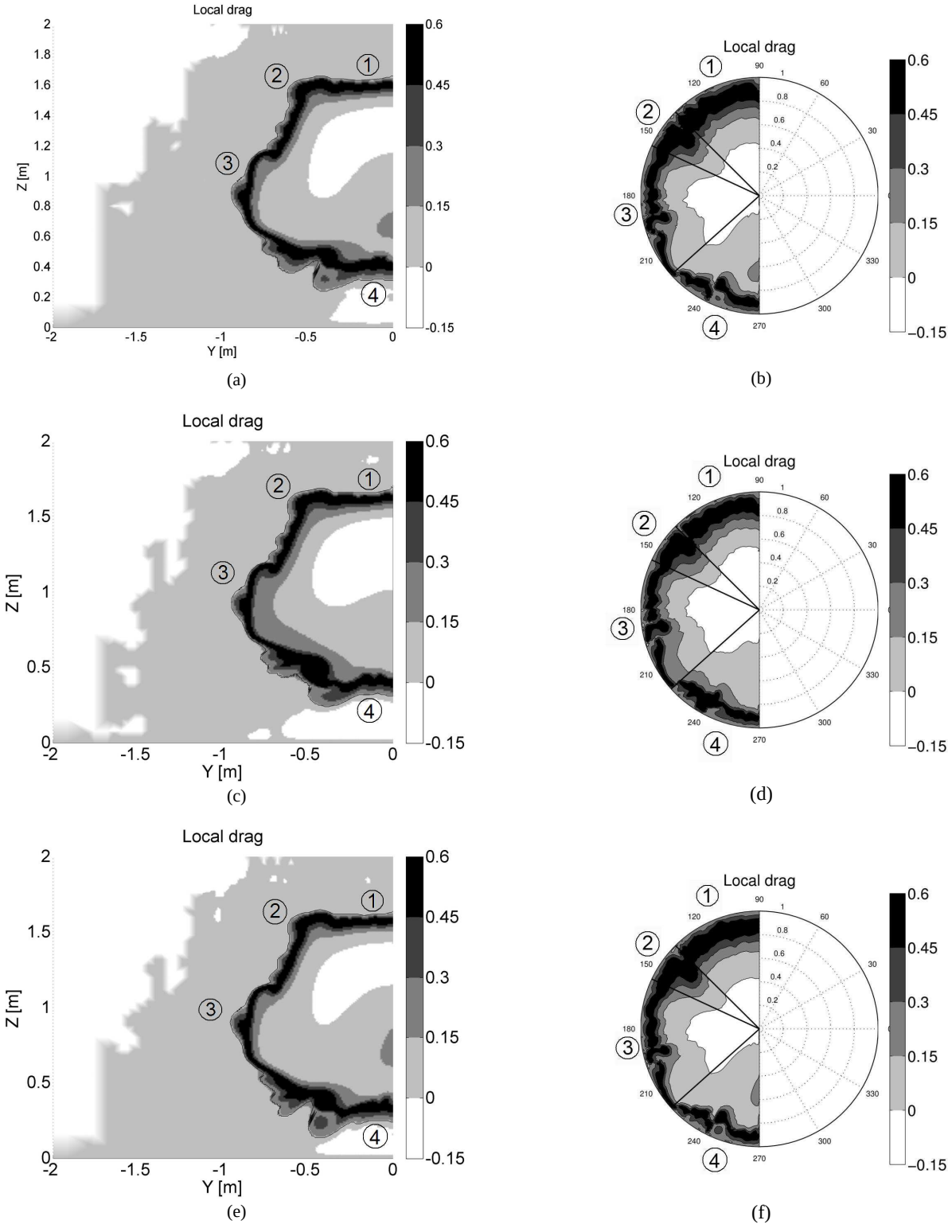

Fig. 6 Local drag of wake plane 100 mm behind the simplified vehicle model. Counterclockwise starting at 90 for the polar plots, the different zones are top wake (1), D-pillar wake (2), side wake (3) and underbody wake (4)

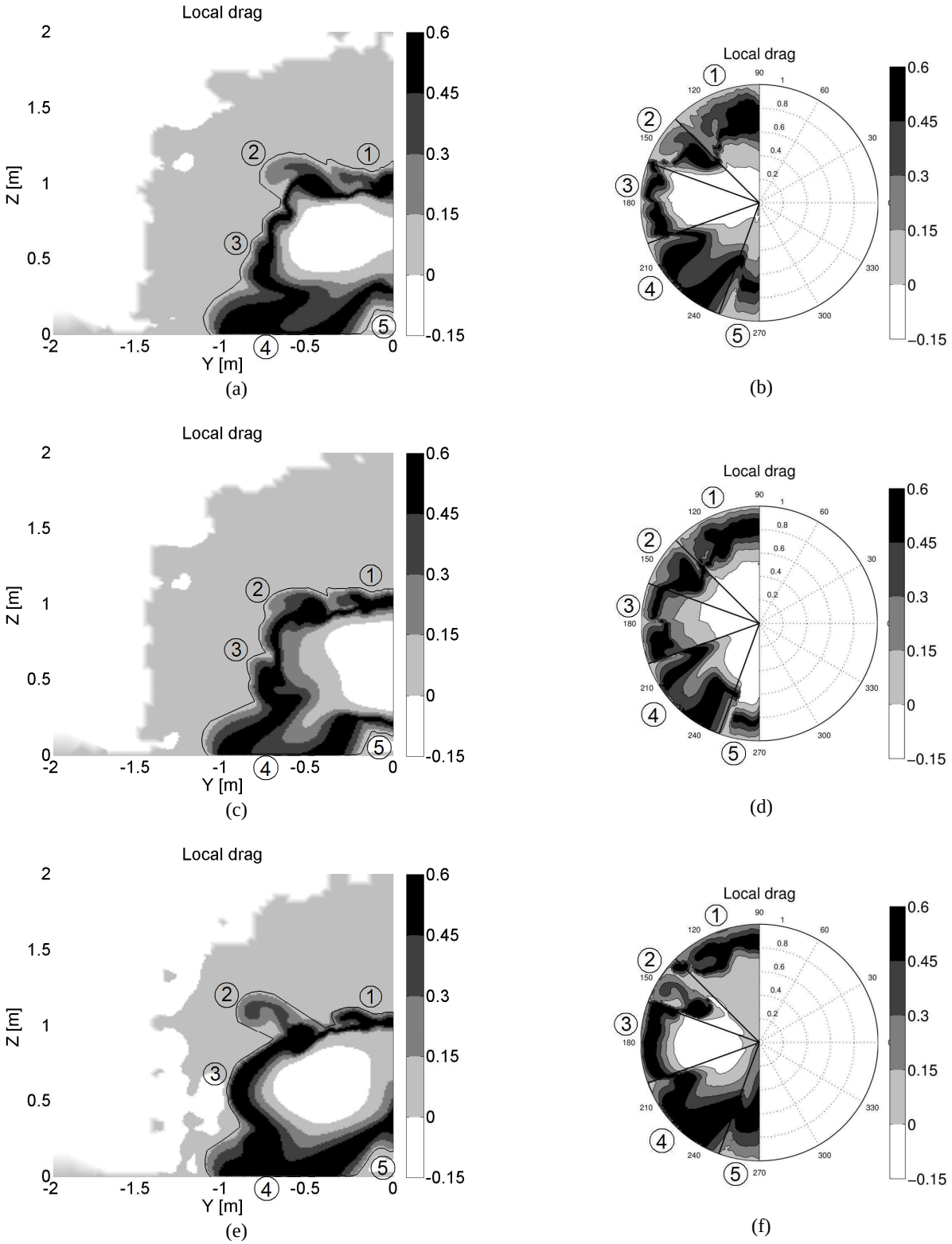

Fig. 7 Local drag of wake plane 100 mm behind the semi-detailed vehicle models. Counterclockwise starting at 90 for the polar plots, the different zones are top wake (1), side mirror wake (2), side wake (3), wheel wake (4) and underbody wake (5)

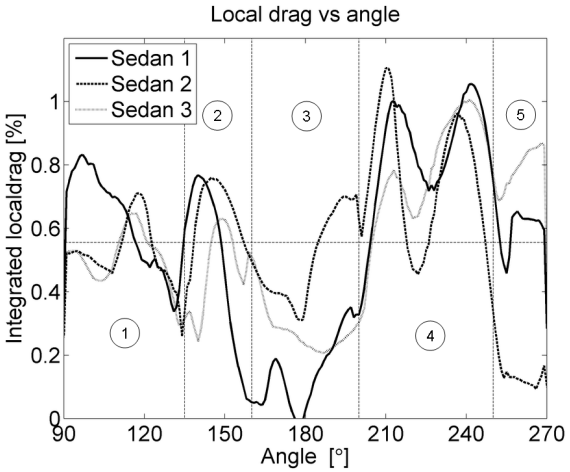

Fig. 8 Piecewise integration local drag of semi-detailed models. The different zones are top wake (1), side mirror wake (2), side wake (3), wheel wake (4) and underbody wake (5).

TABLE III
ΔC_D DETAILED SEDAN MODELS

Model	ΔC_D
Semi – detailed	0.000
Detailed	0.031

The two models show similar flow structure over most of the wake as can be seen by comparing the polar plots of Fig. 7f and Fig. 9, respectively. It can be seen that the largest difference is located in the underbody region. For the detailed model, the local drag near the boundary at the underbody region is much higher. This is caused by the fact that there is less upwash behind the vehicle ensuring a larger wake area and hence less pressure recovery. A secondary effect of the absence of upwash is the change in local drag wake resulting from the side region. changing the overal distribution of the local drag. The division lines at 135º, 160º, 200º and 250º are equal to the ones used in the semi-detailed model. It can be observed that the wheel wake zone for the detailed model shifts 5º clockwise compared to semi-detailed model. The wheel wake now ranges from 155º to 195º.This can be explained by the point of origin in a polar plot (Point 2 in a cartesian plot, see Fig. 5) has a lower z-coordinate in the detailed model. The starting angle for the other drag source, the side mirror wake, is similar for both models, namely 135º. However the end angle is more difficult to see since it's more integrated with the side wake.

In Fig. 10 the integration of the local drag for each degree section as a ratio to the total local drag integration can be seen. For the detailed model, the contribution of the drag sources like wheel wake and side mirror wake, is less pronounced. This implies that the other regions like top wake, side wake and underbody wake are significant contributors to the total local drag. Here, the 5º clockwise shift of the detailed model wheel wake can also be observed and the same conclusion for the side mirror wake as in Fig. 9 can be drawn.

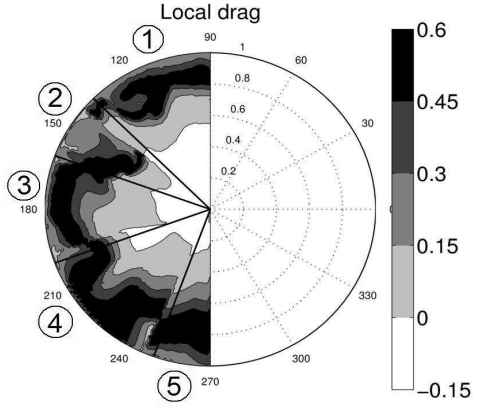

Fig. 9 Polar plot detailed sedan 3. Division in zones as with semi-detailed models

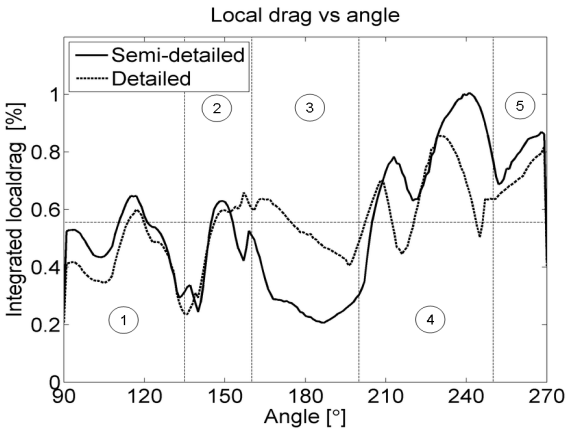

Fig. 10 Piecewise integration local drag of detailed model compared with semi-detailed model. The different zones are top wake (1), side mirror wake (2), side wake (3), wheel wake (4) and underbody wake (5)

With the semi – detailed model, the known drag sources are stronger local drag contributors. This raises the hypothesis that the contribution of the total drag for each section should be as equal as possible (creating an horizontal line) with strong local drag peaks at the intersection between regions of known drag sources, mainly the wheel wake, and regions without a specific drag source, like top region, side region or underbody region.

IV. CONCLUSION

It has been shown in this paper that a conversion to polar plots can contribute to the analysis of bluff body wakes. These polar plots can reproduce the flow structures that are present in the wakes. More over, this representation of the flow structures enables a more clear division of the wake in different sectors. In addition, the integration of the local drag contribution of each sector can be compared to the total integrated local drag. This representation suggests clear distinction between regions of known drag sources and the regions in-between.

In order to obtain a balanced wake these regions should add to the local drag in a uniform way, except perhaps for the wheels. The local drag integration of each degree section as a

ratio to the total local drag of the wake gives an indication that a balanced wake would correspond to a horizontal line. Diversion from this line would be acceptable for locations of known drag sources (not possible to remove), such as the wheels.

Furthermore, it has been shown that the wakes of different car types behave in a similar way, which gives room for direct comparison between different car types.

Future work

The approach presented here is promising to analyse the uniformity of the wake in a more quantitative way. However, it requires further work on different vehicle types. Also, more comparisons have to be conducted where one specific vehicle is investigated with several geometrical changes, both in semi – detailed as well as in fully-detailed configurations. It would also be interesting to examine how a wake would look like in a cartesian plot if the inverse process would be applied on an ideal polar plot.

Acknowledgment

The work discussed in this paper is sponsored by Volvo Car Corporation and VINNOVA. The authors would also like to thank Tim Walker and Christoffer Landström at Volvo Car Corporation for their valuable support.

References

[1] W.H. Hucho, Aerodynamics of Road Vehicles, 4rd ed., United States of America, 1998.
[2] E.C. Maskell, Progress Towards A Method For The Measurement Of The Components Of The Drag Of A Wing Of Finite Span, Royal Aircraft Technical Report, 72232, January 1973.
[3] J.C. Wu, J.E. Hackett and D.E. Lilley, A Generalized Wake-Integral Approach for Drag Determination in Three-Dimensional Flows, AIAA Paper No. 79-0279, New Orleans, January 1979.
[4] S.R. Ahmed, Wake Structures of Typical Automobile Shapes, ASME Journal of Fluids Engineering, Volume 103 (March 1981), Issue 1, pp. 162-169.
[5] M. Onorato, A.F. Costelli and A. Garonne, Drag Measurements Through Wake Analysis, SAE 840302, SAE International Congress and Exposition, Detroit, 1984.
[6] J.E. Hackett and A. Sugavanam, Evaluation of a Complete Wake Integral for the Drag of a Car-Like Shape, SAE 840302, SAE International Congress and Exposition, Detroit, 1984.
[7] S.R. Ahmed, G.Ramm and G. Faltin, Some Salient Features Of The Time-Averaged Ground Vehicle Wake, 840300, SAE International Congress and Exposition, Detroit, USA, 1984.
[8] A. Cogotti, A Strategy For Optimum Surveys of Passenger-Car Flow Field, SAE 890374, SAE International Congress and Exposition, Detroit, USA, 1989.
[9] A. Morelli, A New Aerodynamic Approach to Advanced Automobile Basic Shapes, 2000-01-0491, SAE World Congress, Detroit, USA, 2000.
[10] P. Elofsson, Drag Reduction Mechanisms Due to Moving Ground and Wheel Rotation in Passenger Cars, 2002-01-0531, SAE World Congress, Detroit, USA, 2000.
[11] T. Ivanić and P. Gilliéron, Aerodynamic Drag And Ways To Reduce It, Lecture Series 2005-05, Road Vehicle Aerodynamics, von Karman Institute for Fluid Dynamics, Brussels, Belgium, 2005.
[12] P.B.V. Johansson and W.K. George, The Far Downstream Evolution Of The High Reynolds Number Axisymmetric Wake Behind A Disk, Journal of Fluid Mechanics, Volume 255, pp. 363-385, 2006.
[13] J. Howell, The Decay of Bluff Body Wakes, 2011-01-0178, SAE World Congress, Detroit, USA, 2011.